JOURNAL OF APPLIED ELECTROCHEMISTRY 22 (1992) 38–42

A general computational approach to linear sweep voltammetry at channel electrodes

A. C. FISHER, R. G. COMPTON

Physical Chemistry Laboratory, Oxford University, South Parks Road, Oxford OX1 3QZ, UK

Received 17 March 1991; revised 23 May 1991

A computationally efficient, implicit approach to the simulation of linear sweep and cyclic voltammetry at the channel electrode is derived. The results of computations for a simple reversible electron transfer are presented. First the scan rate requirements for the recording of effective steady state voltammograms are established. Secondly the effect of scan rate upon waveshape and potential shift is described for flow and no flow regimes at the channel electrode. The results are found to be in good agreement with analytical theory where applicable. The ready extension of the method to mechanistically complex schemes is emphasised.

1. Introduction

Channel electrodes are becoming popular well-characterized hydrodynamic electrodes for a wide range of analytical and homogeneous/heterogeneous mechanistic investigations [1]. The main attributes of these cells include the wide range over which mass transport can be varied, operation under chemostatic conditions and the mechanistically discriminating power conferred by the non-uniformity of the diffusion layer over the electrode surface [2].

The purpose of this paper is to provide an efficient implicit computational strategy for the calculation of the current response at a channel electrode, under potential sweep conditions. The method is exemplified with reference to a simple reversible electrode reaction, free of kinetic complications, but is easily modified to allow the description of mechanistically complex systems.

Some approximate analytical theory for linear sweep and cyclic voltammetry at the channel electrode has been derived previously. First, we have presented [3] a theory, valid under conditions where the Lévêque approximation [4] is applicable, showing how the wave-shape and halfwave potential vary with electrode geometry and voltage sweep rate in the limit of slow scan rates. Secondly Singh and Dutt [5–8] have given theory for linear sweep and cyclic voltammetry valid for the full range of interfacial kinetics (reversible, irreversible, quasi-reversible) but their derivations were based on a mathematical simplification in which the concentration gradients in the direction of flow were replaced by their average values. Finally Aoki [9] treated the problem of reversible electron transfer without making assumptions as to the magnitude of the voltage scan rate but again within the Lévêque approximation. However his mathematical treatment is not readily extendable to other mechanistically interesting situations. This restriction is eliminated by the numerical strategy presented here which additionally makes *no* assumptions as to the validity of the Lévêque approximation and is thus valid for electrodes of general geometry and for those flow rates in which the diffusion layer is not confined to being very close to the electrode surface i.e. conditions under which the cell approaches thin-layer characteristics. In all cases the results from our numerical simulations are shown to be in good agreement – under the appropriate conditions – with existing theory.

2. Theory

We consider a simple reversible one electron transfer reduction carried out at a channel electrode at which the potential is swept at a scan rate $v\,\mathrm{V\,s^{-1}}$ from a value at which no current flows to one corresponding to the transport-limited reduction of a species, A:

$$A + e^- \rightleftharpoons B$$

The general convective-diffusion equation describing the distribution of A in time (t) and space is

$$\frac{\partial[A]}{\partial t} = D\frac{\partial^2[A]}{\partial y} - v_x\frac{\partial[A]}{\partial x} \qquad (1)$$

where D is the diffision coefficient of A, the Cartesian-coordinates x and y are as defined in Fig. 1 and v_x is the solution velocity in the x-direction. The velocity components in the y- and z-directions are both zero. If a sufficiently long lead in length exists [10], then the velocity takes the form:

$$v_x = v_0\left(1 - \left(\frac{y'}{h}\right)^2\right) \qquad v_y = 0, \quad v_z = 0 \qquad (2)$$

where h is the half-height of the cell (Fig. 1), $y' = h - y$ and v_0 is the velocity of flow at the centre of the channel.

We assume the electrode potential E_t is swept linearly with time at a rate v, through the reduction wave of A, starting from an initial potential E_i:

$$E_t = E_i - vt$$

0021-891X/92 $03.00 + .12

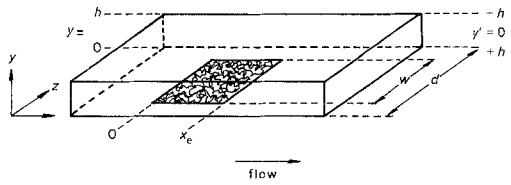

Fig. 1. A schematic diagram of a channel electrode which defines the coordinate system used.

The relevant boundary conditions for reversible electron transfer are:

$$\tau = 0, \quad y \geqslant 0, \quad 0 < x < x_e, \quad [A] = [A]_{bulk}, \quad [B] = 0 \tag{3}$$

$$\tau > 0, \quad y = 0, \quad 0 < x < x_e, \quad \frac{\partial[A]}{\partial y} = -\frac{\partial[B]}{\partial y} \tag{4}$$

$$\tau > 0, \quad y = 0, \quad 0 < x < x_e, \quad \frac{[A]}{[B]} = \theta \exp(-\sigma\tau) \tag{5}$$

$$\text{all } \tau, \quad y = 2h, \quad 0 < x < x_e, \quad \frac{\partial[A]}{\partial y} = \frac{\partial[B]}{\partial y} = 0 \tag{6}$$

where x_e is the electrode length, $[A]_{bulk}$ is the bulk concentration of A,

$$\theta = \exp\left[\left(\frac{F}{RT}\right)(E_i - E^\theta)\right] \tag{7}$$

$$\tau = \left(\frac{9U^2D}{x_e^2h^2}\right)^{1/3} t \tag{8}$$

$$\sigma = (Fv)\left(\frac{x_e^2h^2}{9U^2D}\right)^{1/3} \tag{9}$$

E^θ is the standard electrode potential of the A/B couple and U is the mean solution flow rate (cm s^{-1}). In writing Equation 4 we have assumed A and B to have identical diffusion coefficients. The form of the parameters τ and σ is suggested by the theoretical treatments valid for the Lévêque conditions [3, 9] which show that then the current–voltage curve is solely a function of σ.

Solution of Equations 1–6 may be achieved by the use of a two-dimensional finite difference grid which covers the x–y plane, as shown in Fig. 2. Spacings in the two directions are Δx and Δy, respectively, so that

$$\Delta x = \frac{x_e}{K}$$

$$\Delta y = \frac{2h}{J}$$

We may then define concentrations at a point (j, k) corresponding to $x = k\Delta x$, $y = j\Delta y$. We use the symbol $a_{j,k}$ to denote the concentration of A at this point.

Equations 1 and 2 may be then cast into finite-difference form if we define the parameters

$$\lambda_j^c = \frac{6V_f\Delta y\,\Delta t\,j(2h - j\Delta y)}{d(2h)^3\Delta x} \tag{10}$$

and

$$\lambda^y = \frac{D\Delta t}{(\Delta y)^2} \tag{11}$$

where $V_f(=4v_0dh/3 = 2Uhd)$ is the volume flow rate. Δt represents an increment of time. We use the notation ${}^ta_{j,k}$ to indicate the concentration of A at time $t\Delta t$. Equation 1 then becomes

$$\frac{{}^{t+1}a_{j,k} - {}^ta_{j,k}}{\Delta t} = \frac{D}{(\Delta y)^2} \times \{{}^{t+1}a_{j-1,k} - 2{}^{t+1}a_{j,k} + {}^{t+1}a_{j+1,k}\} - v_x\left\{\frac{{}^{t+1}a_{j,k} - {}^{t+1}a_{j,k-1}}{\Delta x}\right\} \tag{12}$$

Or, rearranging

$${}^ta_{j,k} + \lambda_j^c\{{}^{t+1}a_{j,k-1}\} = -\lambda^y\{{}^{t+1}a_{j-1,k}\} + (2\lambda^y + \lambda_j^c + 1)\{{}^{t+1}a_{j,k}\} - \lambda^y\{{}^{t+1}a_{j+1,k}\} \tag{13}$$

Application of the boundary condition (5) gives

$${}^ta_{1,k} + \lambda_1^c\{{}^{t+1}a_{1,k-1}\} + \frac{\lambda^y\theta\exp(-\sigma(t+1)\Delta\tau)}{1. + \theta\exp(-\sigma(t+1)\Delta\tau)} = (2\lambda^y + \lambda_1^c + 1)\{{}^{t+1}a_{1,k}\} - \lambda^y\{{}^{t+1}a_{2,k}\} \tag{14}$$

while the boundary condition (6) results in

$${}^ta_{J-1,k} + \lambda_{J-1}^c\{{}^{t+1}a_{J-1,k-1}\} = -\lambda^y\{{}^{t+1}a_{J-2,k}\} + (\lambda^y + \lambda_{J-1}^c + 1)\{{}^{t+1}a_{J-1,k}\} \tag{15}$$

Systems of equations of the form of those in Equations 13–15 may be expressed in the form of a $(J-1) \times (J-1)$ tridiagonal matrix as described in [11]. Specifically

$$\{\boldsymbol{d}\} = [\boldsymbol{T}]\{\boldsymbol{u}\} \tag{16}$$

where

$$\begin{bmatrix} d_1 \\ d_2 \\ \vdots \\ d_j \\ \vdots \\ d_{J-2} \\ d_{J-1} \end{bmatrix} = \begin{bmatrix} b_1 & c_1 & 0 & & & & \\ a_2 & b_2 & c_2 & 0 & & & \\ & \ddots & \ddots & \ddots & & & \\ & 0 & a_j & b_j & c_j & 0 & \\ & & & \ddots & \ddots & \ddots & \\ & & & & a_{J-2} & b_{J-2} & c_{J-2} \\ & & & & 0 & a_{J-1} & b_{J-1} \end{bmatrix} \begin{bmatrix} u_1 \\ u_2 \\ \vdots \\ u_j \\ \vdots \\ u_{J-2} \\ u_{J-1} \end{bmatrix}$$

The matrix elements are given by:

$k = 1$,

$$d_1 = {}^ta_{1,1} + \lambda_1^c + \frac{\lambda^y\theta\exp(-\sigma(t+1)\Delta\tau)}{(1. + \theta\exp(-\sigma(t+1)\Delta\tau)} \tag{17}$$

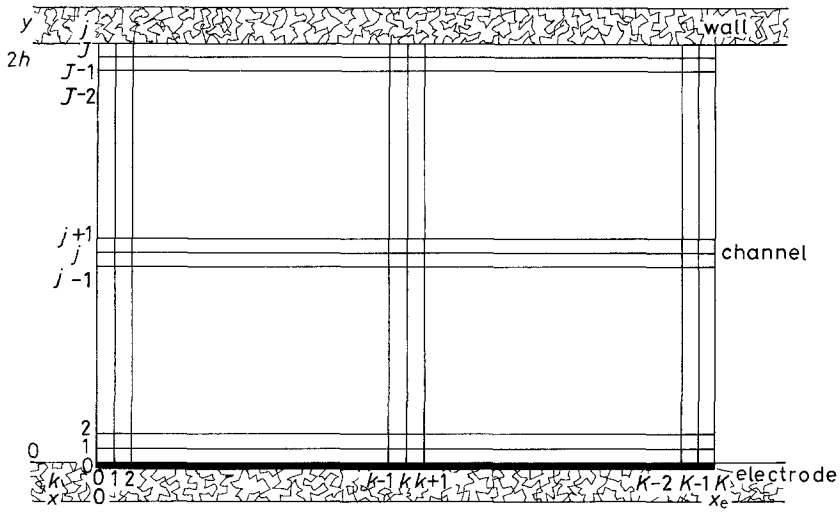

Fig. 2. The finite difference grid used as the basis for the numerical calculations.

$$d_j = {}^{t}a_{j,1} + \lambda_j^c \qquad j = 2, 3 \ldots J-1 \qquad (18)$$

$k > 1$

$$d_1 = \{{}^{t}a_{1,k}\} + \lambda_1^c\{{}^{t+1}a_{1,k-1}\} + \frac{\lambda^y\theta \exp(-\sigma(t+1)\Delta\tau)}{(1. + \theta \exp(-\sigma(t+1)\Delta\tau)} \qquad (19)$$

$$d_j = \{{}^{t}a_{j,k}\} + \lambda_j^c\{{}^{t+1}a_{j,k-1}\} \qquad j = 2, 3 \ldots J-1 \qquad (20)$$

$$b_j = 2\lambda^y + \lambda_j^c + 1 \qquad j = 1, 2 \ldots J-2 \qquad (21)$$

$$u_j = {}^{t+1}a_{j,k} \qquad j = 1, 2 \ldots J-1 \qquad (22)$$

$$c_j = -\lambda^y \qquad j = 1, 2 \ldots J-1 \qquad (23)$$

$$a_j = -\lambda^y \qquad j = 1, 2 \ldots J-1 \qquad (24)$$

$$b_{J-1,k} = \lambda^y + \lambda_{J-1}^c + 1 \qquad (25)$$

Note that the matrix Equation 16 shows how the concentrations throughout the cell at time $(t + 1)\Delta t$ may be calculated if we know those at time $t\Delta t$. To do this we have to find the set of vectors $\{\boldsymbol{u}\}$: for each k value has its own vector $\{\boldsymbol{u}\}_k$. The matrix $[\boldsymbol{T}]$ being of tridiagonal form allows us to use the Thomas algorithm [11] to give $\{\boldsymbol{u}\}_k$ from $\{\boldsymbol{d}\}_k$. The boundary condition 3 supplies the vector $\{\boldsymbol{d}\}_0$ from which $\{\boldsymbol{u}\}_0$ is calculated. Then $\{\boldsymbol{d}\}_{k+1} = \{\boldsymbol{u}\}_k$, so $\{\boldsymbol{u}\}_1$ is calculated from $\{\boldsymbol{d}\}_1$, and so on until $\{\boldsymbol{u}\}_k$ is obtained. The calculation is then repeated.

In this way the concentration profile of A within the flow cell may be calculated as a function of time. The current at the electrode may thus be evaluated at any instant from

$${}^{t}I = wFDa_0\left\{\sum_{k=1}^{K}({}^{t}a_{1,k} - {}^{t}a_{0,k})\frac{\Delta x}{\Delta y}\right\} \qquad (26)$$

Using the theory outlined above linear sweep voltammetric transients were computed (on a Sun IPC Sparc work station) and convergence examined by varying J, K and Δt values. The simulations employed the following general parameters, unless specified as different in the text below, $2h = 0.04\,\text{cm}$, $d = 0.6\,\text{cm}$, $x_e = 0.4\,\text{cm}$, $w = 0.4\,\text{cm}$ and for a diffusion coefficient of $D = 1 \times 10^{-5}\,\text{cm}^2\,\text{s}^{-1}$. To achieve convergence values of $K = 200$ and $J = 200$ were required to give convergence to 3 significant figures. Values of Δt in the range 0.05–0.002 s gave identical results for scan rates in the range $0.5 > v > 0.00005\,\text{V s}^{-1}$.

The theory is simply extended for the case of cyclic hydrodynamic voltammetry, that is where the scan is reversed so as to 'see' the reconversion of B to A. In this case the simulation is exactly the same as the approach above on the forward scan. However for computation of the reverse sweep the electrode potential is given by

$$E_t = E_F + v(t - t^*)$$

where E_F is the potential at which the forward scan is reversed at time t^*.

3. Results and discussion

Preliminary computations were undertaken to test the predictions of the new approach at infinitesimally slow scan rates against the behaviour computed directly for steady state conditions from the appropriate boundary conditions [11]. Figure 3 shows the current (normalized to the steady state limiting current) response of a steady state calculation using a flow rate V_f of $1 \times 10^{-2}\,\text{cm}^3\,\text{s}^{-1}$ for the electrode geometry specified above, together with that predicted for a scan rate of $0.0005\,\text{V s}^{-1}$ using the new approach. As can be seen excellent agreement is observed supporting our general computational approach. In addition analytical theory predicts that, under conditions where the Lévêque approximation holds, the current voltage response should be a unique function of the parameter σ [3, 9]. This prediction was verified by varying the scan rate and flow rate over wide ranges. The results of this are exemplified by Fig. 4 which shows two superimposed normalized current/voltage plots both calculated for a fixed value of $\sigma = 0.62$ and generated by varying scan rate from 0.1 to $0.01\,\text{V s}^{-1}$ and altering the flow rate appropriately (Equation 9). Excellent consistency is observed – the curves agree to better than ± 1% over the whole range – indicating, again, that our computations are in

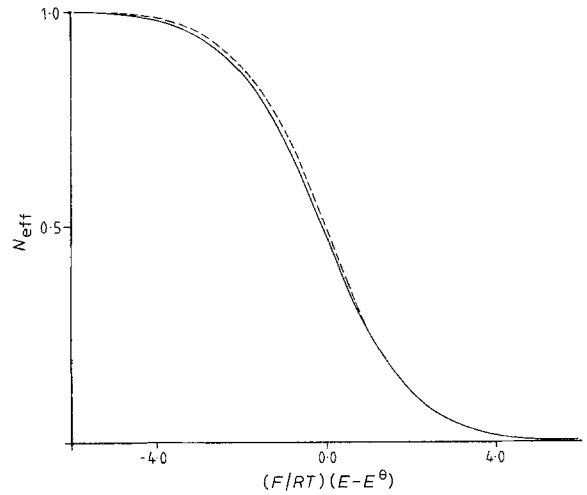

Fig. 3. Current–voltage curves calculated for the electrode of geometry specified in the text with a solution flow rate of 10^{-2} cm^3 s^{-1}. The solid line shows the behaviour calculated for true steady state conditions [11] and the dotted line that for a scan rate of 0.0005 V s^{-1} using the new computational approach. N_{eff} describes the current normalized to the steady state limiting current.

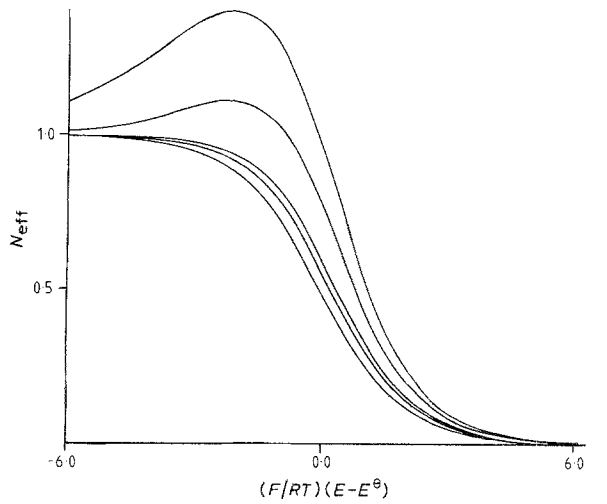

Fig. 5. The variation of the normalized current–voltage waveshape with different scan rates for the electrode geometry and electrolyte flow rate as specified in the text. The scan rates used were 0.5, 0.2, 0.06, 0.03 and 0.005 V s^{-1}. The faster the scan rate, the more pronounced is the current maximum. A curve calculated for a scan rate of 0.0005 V s^{-1} was indistinguishable when plotted from that shown in the figure for 0.005 V s^{-1}.

good limiting agreement with analytical theory. As a final preliminary check attention was focused on the predicted cyclic voltammetric behaviour under conditions of *no* flow in the cell geometry given above. The variation of peak height with scan rate was analysed and showed the expected square root behaviour and peak-to-peak separation of conventional, unbounded cyclic voltammetry [9]. The validity of the general numerical approach was thus established as verified.

We next employ the simulation method in a new range of essentially unexplored channel electrode problems. The first effect investigated was the apparent shift in potential of the current–voltage curve with scan rate. As the scan rate is increased slow diffusion in solution causes the concentration profile of A to 'lag behind' its true steady state distribution so that a peak appears in the current–voltage curve. At the same time the wave becomes shifted from that observed under scan rates sufficiently slow so as to allow a true steady state to be established. Figure 5 shows a typical plot of the waveshape and potential shift for a flow rate of 5.211×10^{-2} cm^3 s^{-1}. The appropriate scan rates are defined in the figure legend. The wave is seen to shift anodically with scan rate and the potential shift was found to be in good quantitative agreement with that predicted from analytical theory [3].

Next simulations were performed for cyclic voltammetry and the effect of shrinking the channel height to approach thin-layer cell conditions examined via the shape of the voltammograms predicted. For these simulations a value of $2h = 0.0005$ cm and scan rate of 0.005 V s^{-1} were employed; otherwise the cell parameters were as defined above. The results obtained are presented in Fig. 6. Curve (a) was obtained under

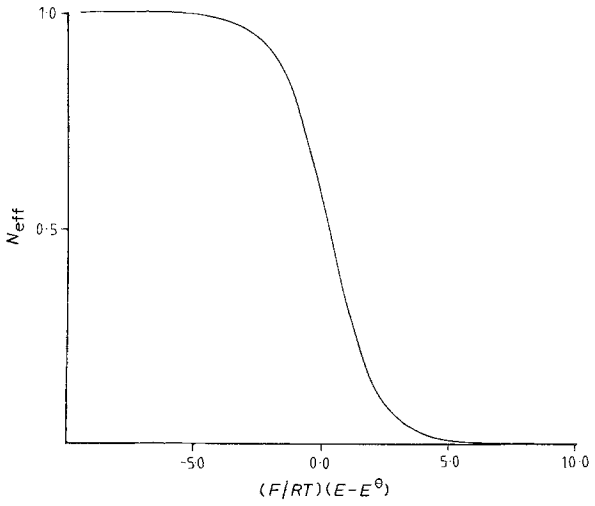

Fig. 4. Current–voltages curves computed for the electrode of Lévêque geometry (specified in the text) for differing voltage scan rates and solution flow rates such that the parameter σ is fixed at the value 0.62.

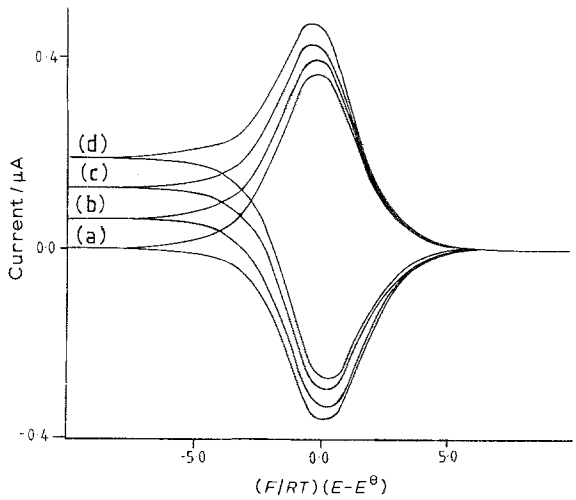

Fig. 6. Current–voltage curves generated for a thin layer channel electrode cell (see text) for flow rates of V_f = (a) 0; (b) 10^{-6}; (c) 10^{-5} and (d) 2×10^{-5} cm^3 s^{-1}. The higher the flow rate the greater the steady-state limiting reduction current.

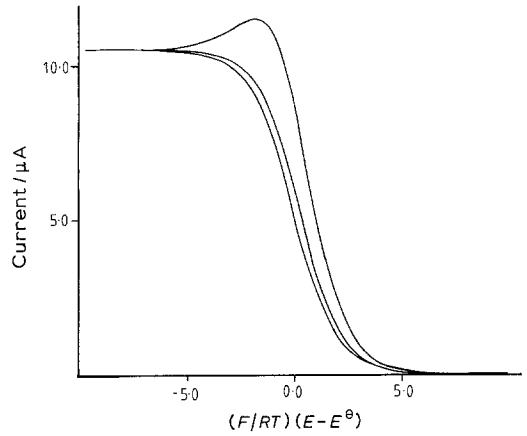

Fig. 7. Current–voltage curves showing the influence of scan rate on the waveshape measured at a channel electrode of the dimensions given in the text and for a solution flow rate of 5×10^{-4} cm^3 s^{-1}. The three curves relate to voltage scan rates of 0.000 05, 0.0005 and 0.005 V s^{-1}.

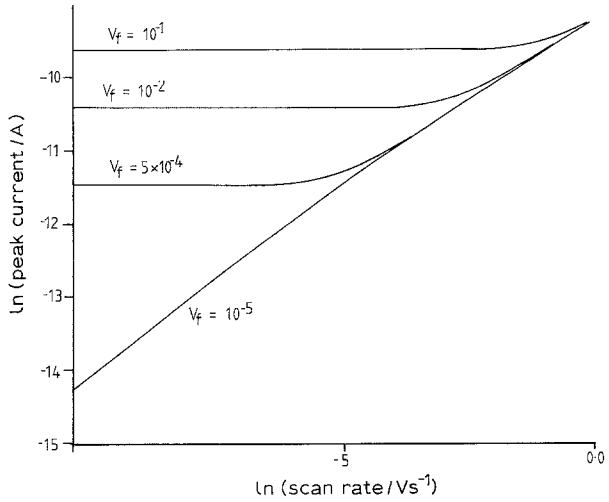

Fig. 8. A working curve summarizing the results of calculations such as presented in Fig. 7 showing the transition between pure steady-state hydrodynamic and pure diffusional behaviour for a series of flow rates (V_f/cm^3 s^{-1}).

conditions of no flow and the resulting current–voltage peak is symmetrical, as expected. With the introduction of flow (Fig. 6b–d) the forward and reverse peaks become asymmetric and the reverse peak current reduced in intensity, approaching the behaviour expected for ordinary flow rates and geometries.

Attention was then returned to conventional cell geometries, and the criteria for the experimental measurement of steady state voltammograms established. A wide range of flow rates and scan rates was investigated. Figure 7 presents typical current–voltage curves calculated from the simulations. At slow scan rates the maximum current observed in the simulations is that of the normal transport limiting current. However as one scans progressively faster a peak appears in the current (Fig. 7) and ultimately, at relatively fast scan rates, this peak current tends to the behaviour of a purely diffusional regime. This is best illustrated by a plot of log(peak current) against log(scan rate) as depicted in Fig. 8 for a series of flow rates. It can be seen that at fast scan rates a slope of 1/2 is observed corresponding to the purely diffusional limit, whereas at slow scan rates the peak current is scan rate independent. Plots such as Fig. 8 are important in that they define the range of scan rates permissible to the experimentalist for given electrode parameters so that authentic steady state current–voltage curves may be obtained, for example for Tafel, or other, analysis.

In conclusion, we have developed a general efficient and simple computational approach for the solution of the time dependent problems at the channel electrode. This should make this highly advantageous electrode design accessible for a much wider range of applications.

Acknowledgement

We thank Mark Latham for interesting discussions.

References

[1] P. R. Unwin and R. G. Compton, *Comprehensive Chemical Kinetics* **29** (1989) 173.
[2] R. G. Compton, A. C. Fisher and G. P. Tyley, *J. Appl. Electrochem.* **21** (1991) 295.
[3] R. G. Compton and P. R. Unwin, *J. Electroanal. Chem.* **206** (1986) 57.
[4] M. A. Lévêque, *Ann. Mines Mem. Ser. 12* **13** (1928) 201.
[5] T. Singh and J. Dutt, *J. Electroanal. Chem.* **182** (1985) 259.
[6] *Idem, ibid.* **190** (1985) 65.
[7] *Idem, ibid.* **196** (1985) 35.
[8] *Idem, ibid.* **207** (1986) 41.
[9] K. Aoki, K. Tokuda and H. Matsuda, *ibid.* **209** (1986) 247.
[10] R. G. Compton and B. A. Coles, *ibid.* **144** (1983) 87.
[11] R. G. Compton, M. B. G. Pilkington and G. M. Stearn, *J. Chem. Soc. Faraday Trans. I* **84** (1988) 2155.